*Proc. Lunar Sci. Conf. 6th* (1975), p. 3557–3576.
Printed in the United States of America

# Long-term differential energy spectrum for solar-flare iron-group particles

G. E. BLANFORD

The Lunar Science Institute, Houston, Texas 77058

R. M. FRULAND and D. A. MORRISON

NASA Johnson Space Center, Houston, Texas 77058

**Abstract**—Track density profile measurements in sample 64455 and sample 68815 have been used to derive a long-term solar-flare differential energy spectrum for iron-group ($20 \leqslant Z \leqslant 26$) nuclei from ~0.1 to ~600 MeV/a.m.u. In 64455, quench crystals of plagioclase permitted measurements from uneroded surfaces, the microcrater distribution indicated that the rock had a simple exposure history, and the sample exposure age of $2.01 \pm 0.1 \times 10^6$ yr was determined by the $^{81}$Kr–Kr method (Marti, personal communication). The data for 68815 came from Walker and Yuhas (1973). The energy spectrum which generates the best fit to the normalized track densities is a power law of the form $4.9 \times 10^{10} E^{-1.4}$ from ~0.1 to ~15 MeV/a.m.u. which smoothly connects to a power law of the form $7.4 \times 10^{12} E^{-3}$ from ~35 to 70 MeV/a.m.u. Finally the spectrum smoothly connects to a modulated galactic cosmic-ray spectrum similar to that measured near solar maximum during solar cycle 20. Standard track production versus depth profiles can be used to determine solar-flare track exposure ages and erosion rates for lunar samples.

## INTRODUCTION

INTERPRETING TRACK DENSITIES in the upper several millimeters of a lunar rock requires accurate knowledge of track production profiles (track density versus depth) at these depths. With a standard track profile, measured track profiles can be used to determine exposure ages and erosion rates on lunar surfaces. Solar-flare iron-group ($20 \leqslant Z \leqslant 26$) particles dominate track production up to several millimeters depth in lunar rocks with the track production profile being a strong function of the differential energy spectrum of the solar-flare particles. Because lunar surfaces exposed to solar-flare particles are also exposed to micrometeor bombardment, it has been difficult to find uneroded lunar samples from which to measure the track production profile. Initially the solar-flare track profile measurement from a glass filter on the Surveyor 3 camera was used to derive a solar-flare differential energy spectrum for iron-group nuclei and a standard track production profile (Crozaz and Walker, 1971; Fleischer *et al.*, 1971; Price *et al.*, 1971). This derivation posed many problems such as determination of the track etching efficiency of the glass, determination of the magnitude of the correction required in extrapolating the 2.6-yr Surveyor exposure period to the long-term average, and the uncertainty in spectral shape because of the few, relatively small flares sampled. A significant improvement was made in the energy regime from 100 to 600 MeV/a.m.u. where the solar and galactic source particles

overlap with the measurement of the track profile by Walker and Yuhas (1973) in sample 68815 for which an exposure age was accurately measured by the $^{81}$Kr–Kr method (Behrman *et al.*, 1973). This sample was not satisfactory for determining the spectrum at lesser depths because the measured track profile clearly indicated, by its flattened slope, that sample 68815 had suffered significant erosion. Hutcheon *et al.* (1974) complemented the work on 68815 by measuring the track profile in a specially shielded sample from rock 72315 which enabled them to calculate the differential energy spectrum from 1 MeV/a.m.u. to several hundred MeV/a.m.u.

Here we present measurements of the track production profile in lunar sample 64455. This analysis has several advantages over the analysis of sample 72315 because: (1) the exposure age of 64455 was determined by krypton isotope analysis providing independent calibration of track production and (2) no correction for galactic cosmic-ray tracks superposed in the solar-flare region is required. Portions of the surface of 64455 are uneroded which permitted the determination of the track production profile up to a depth of 700 $\mu$m (~40 MeV/a.m.u.). But beyond this depth (see Fig. 1) the existence of pits and spall zones affected track densities and the track production profile is inferred by smoothly connecting the curve to agree with the measurements in sample 68815 (Walker and Yuhas, 1973).

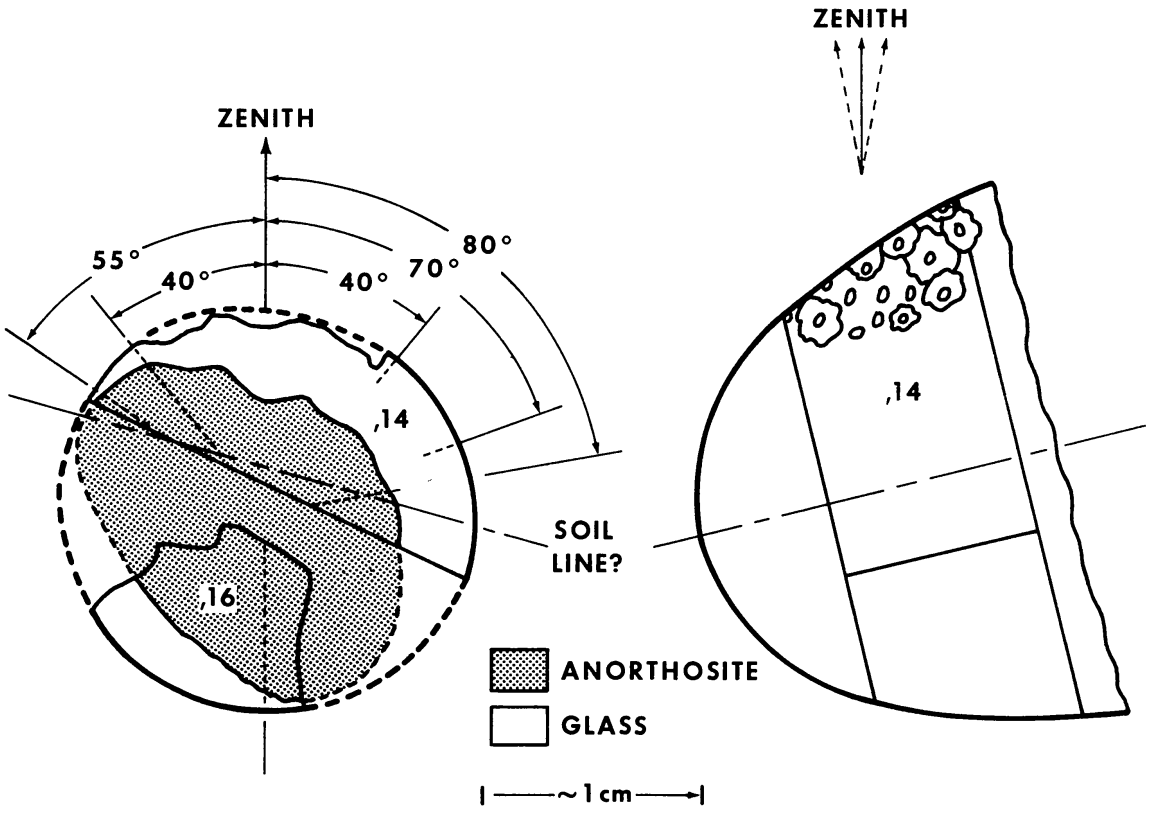


Fig. 1. A sketch of lunar sample 64455 in its supposed lunar orientation determined from its distribution of microcraters. Daughter samples 64455,14 and 64455,16 are shown as determined from cutting photographs taken by the curatorial staff. Dotted lines represent radii along which track density profiles were measured.

The analysis of both samples enables us to determine the long-term differential energy spectrum for iron-group nuclei from ~0.1 to ~600 MeV/a.m.u.

## Experimental Method and Analysis

Lunar rock 64455 has a number of special properties which make it especially suitable for track studies. It is an anorthosite with a glass coating in which a rind of quenched plagioclase crystals formed. The quench crystals and the smooth external shape of the coating provide incontrovertible evidence of noneroded surfaces and, in addition, the crystals are an excellent medium in which to do track analysis. The distribution of pits and microcraters, restricted to the top surface, indicate that the rock was not overturned or otherwise seriously disturbed between ejection and sampling. Finally, the $^{81}$Kr–Kr exposure age of the glass has been determined to be $2.01 \times 10^6$ yr ± 5% (Marti, personal communication). This age and the rock's chemical composition place it among the well-dated South Ray Crater ejecta with a weighted average exposure age of $2.03 \pm .06 \times 10^6$ yr (based on Marti's measurement and Drozd *et al.*, 1974). Figure 1 is a sketch of sample 64455 which shows its position on the lunar surface determined from the distribution of microcraters by Schneider and Hörz (1974) and ourselves. The zenith is chosen to correspond to the center of the most intensely eroded areas and the soil line is chosen to lie along the points where there is no evidence of microcratering. The positions of 64455,14 and 64455,16, in which we measured track densities, are shown as determined from cutting photos taken by the curatorial staff. A petrologic description of 64455 is given by Blanford *et al.* (1974).

We etched samples containing plagioclase crystals in a boiling solution of NaOH initially at 1 N with 5 ml/l of Kodak Photoflo 200 solution added as a wetting agent. Unfortunately, we have recently learned that the solution slightly evaporated during long etching runs and consequently, identical etching times performed in a different number of steps do not correspond to the same degree of track development.

In Fig. 2 we have graphed the raw data of track density measurements in lunar rock 64455. Table 1 gives the meaning of the different symbols used in Fig. 2 and 3. From the zenith angle given in Table 1 and the letter L (left) and R (right) the corresponding radius along which measurements were made can be seen in Fig. 1. Because measurements were made along different radii and represent different degrees of track development (i.e. etch times), the data points in Fig. 2 do not form a smooth curve. Therefore, we determined, by the method of least squares, the best power law fit to each data set (the upper three points marked as closed triangles were excluded from the power law fit for the reasons given by Blanford *et al.* (1974). These data sets were then normalized to each other and then normalized to the set measured optically and represented in Fig. 2 by solid diamonds. The normalized data are shown in Fig. 3. We believe that the normalization requirement arises from two factors which depend upon zenith angle and the degree of track development. Table 1 gives the total normalization factor for each data set and shows the normalization component attributed to

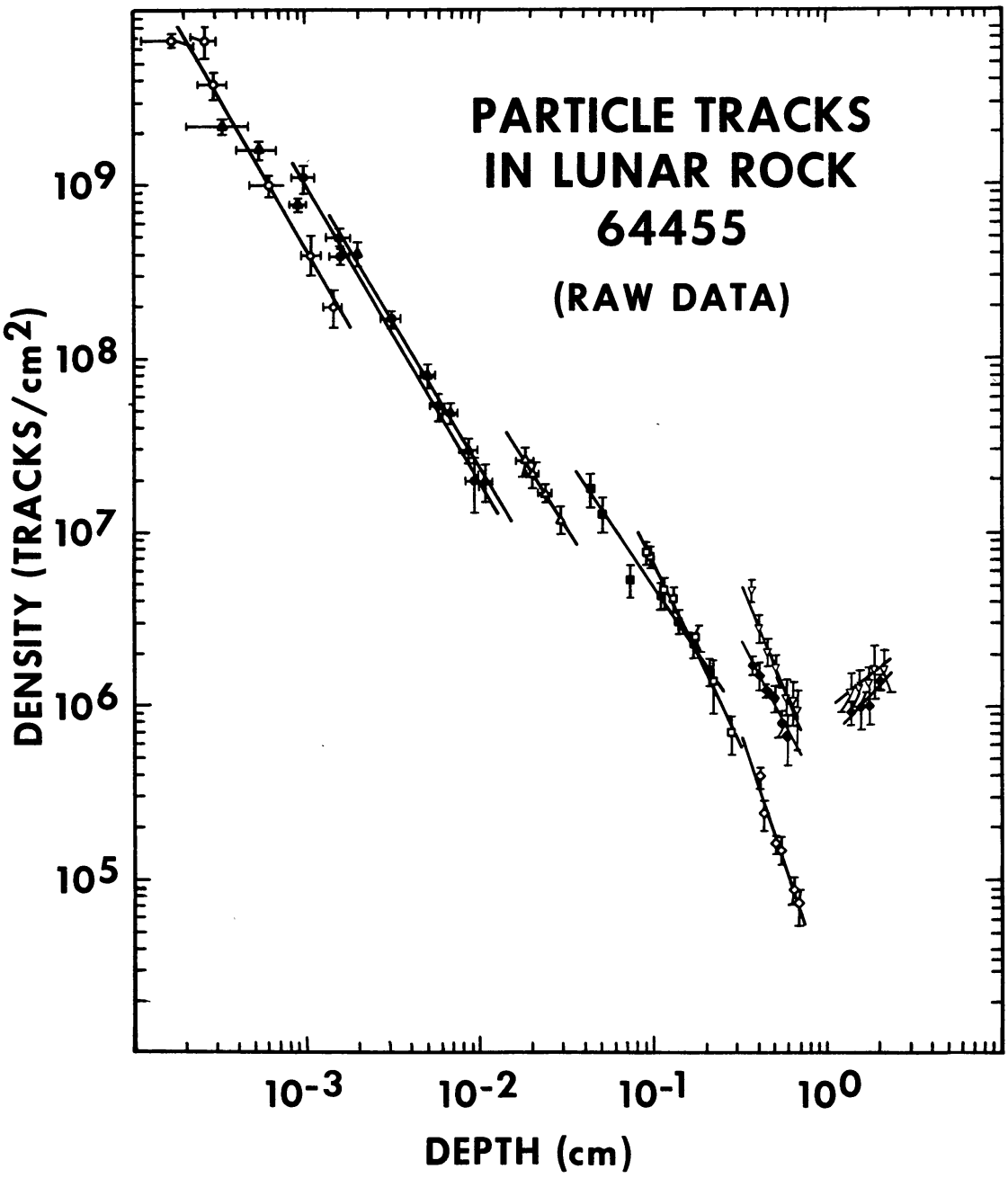


Fig. 2. Densities of solar-flare particle tracks at different depths in sample 64455. The meaning of the different symbols is given in Table 1. The line segments represent least-square fits to the data groups.

differences in zenith angle (determined from Fig. 9 below) and the component attributed to differences in the degree of track development which is best expressed as a difference in $\overline{\Delta R}$, a term which will be discussed in the following section.

Most other groups have not found it necessary to normalize data taken under different etching and observing conditions and therefore we must justify this

1975LPSC....6.3557B



Table 1. Symbols used in Figs. 2 and 3.

| Symbol | Etching time (hr) | Observing instrument | Magnification | Zenith angle | Slope | Total normalizing factor | Normalizing factor from zenith angle to 80° | Normalizing factor attributed to changes in $\overline{\Delta R}$ | Estimated $\overline{\Delta R}$ ($\mu$m) |
|---|---|---|---|---|---|---|---|---|---|
| ○ | 0.33<br>2.5 min | SEM | 33,000× | 40°R | −1.75 | 245 | .633 | 387 | .02 |
| ● | 6 g NaOH<br>8 g $H_2O$ | SEM | 10,000× | 60°R | −1.7 | 104 | .774 | 134 | .07 |
| ▲ | 0.66 | SEM | 11,500× | 70°R | −1.7 | 86.7 | .889 | 97.5 | .09 |
| △ | 1.0 | SEM | 3,400× | 40°L | −1.6 | 29.0 | .633 | 45.8 | 0.2 |
| □ | | | | 55°L | −1.5 | 8.08 | .728 | 11.1 | 0.8 |
| | 6 | SEM | 3,400× | | | | | | |
| ■ | | | | 40°L | −2.1 | 7.23 | .633 | 11.4 | 0.8 |
| ◇ | 9 | Optical | 1,250× | 80°R | −3.0 | 7.18 | 1 | 7.18 | 1.2 |
| | <1 cm | | | 80°R | −2.0 | 1 | 1 | 1 | 9 |
| ◆ | 9.4 | Optical | 1,600× | | | | | | |
| | >1 cm | | | 0° | 1.0 | .555 | .555 | 1 | 9 |
| | <1 cm | | | 80°R | −2.4 | .549 | 1 | .549 | 16 |
| ▽ | 3.4 | SEM | 5,800× | | | | | | |
| | >1 cm | | | 0° | 0.8 | .248 | .555 | .447 | 20 |
| ▼ | Averages of data shown in Fig. 2 as solid diamonds and normalized values of open "inverted" triangles when the data were measured at the same location. | | | | | | | | |

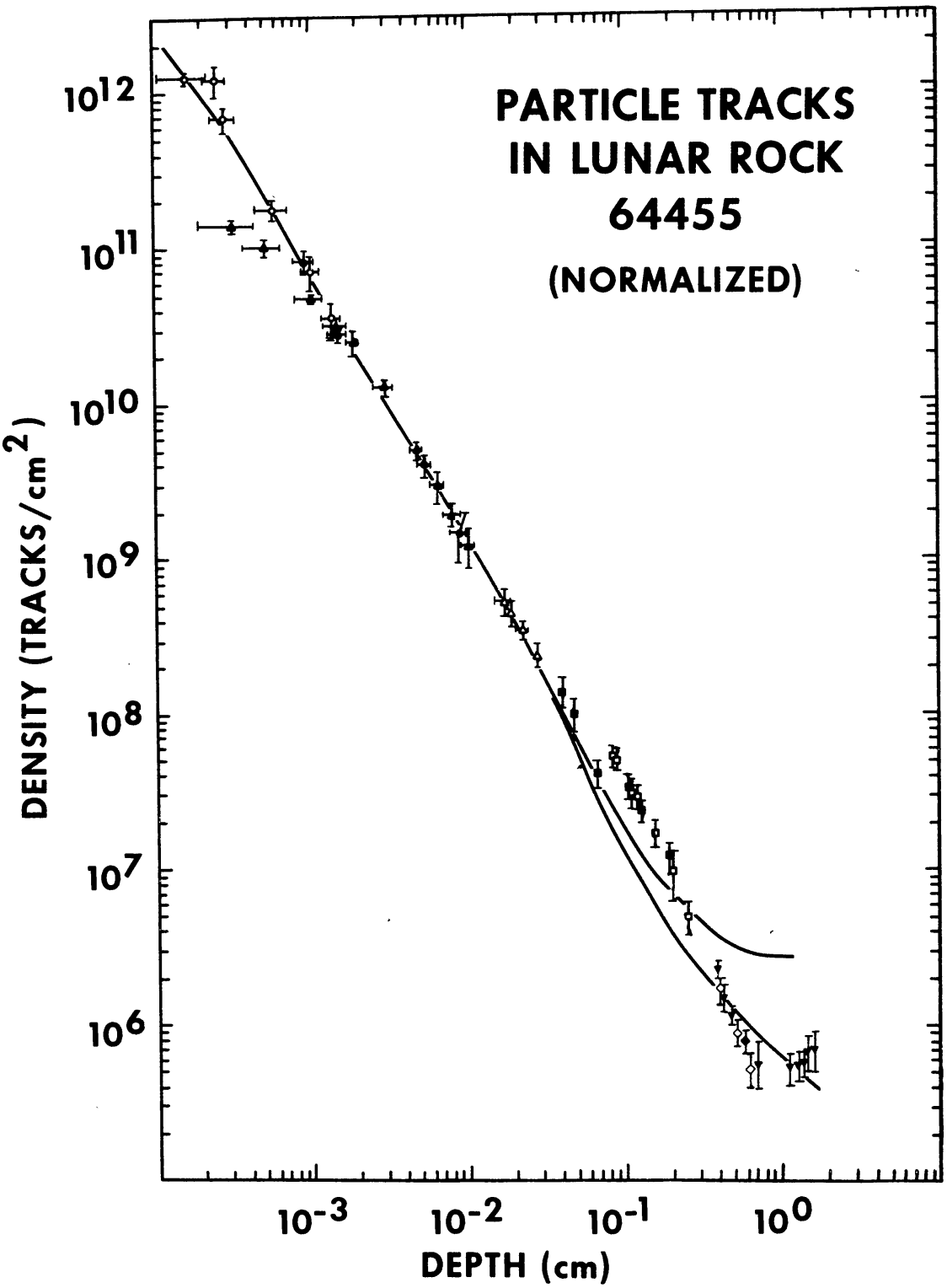


Fig. 3. Normalized densities of solar-flare particle tracks at different depths in sample 64455. The meaning of the different symbols is given in Table 1. The lines represent the track density profiles derived from Eq. (2) where the upper line is for a radius of curvature of 0.9 cm and the lower line is for an infinite plane rock surface.

procedure. We observe that track densities increase with increasing etching time until track lengths typical of optical observations are achieved. We have observed increases in track density in the same areas observed successively with increasing etching time. Some points shown as solid diamonds and open inverted triangles in Fig. 2 correspond to the same area observed at different times and etched for different periods and an increase in track density with longer etching time is clearly indicated (most of our measurements, however, were not taken from the same areas in the course of successive etches). We also observe, as do Crozaz *et al.* (1971), that track densities determined optically are approximately one half the densities determined by SEM when both measurements are made on the same crystal.

To determine whether or not the requirement for normalization was peculiar to sample 64455, we measured track densities in rock 76215. This sample was catastrophically removed from Boulder 4, Station 6 of the Apollo 17 site (ALGIT, 1973) and fresh surfaces were exposed for a short period ($1\text{–}2 \times 10^4$ yr). The rock has very low microcrater densities (Morrison and Zinner, 1975) and virtually uneroded surfaces. Figure 4 shows the measured track densities, both uncorrected and corrected for the galactic background. Track density points in Fig. 4 with the same abscissa values are repeat measurements of the same locations. As shown in Fig. 4, two SEM data sets representing differing etch times (and therefore differing degrees of track development) and different magnifications on the SEM are offset and we conclude that the lower density data set should be normalized to the higher. Figure 5 shows SEM photographs used to measure one location under differing conditions of etch time and magnification, and it is clear that the track density in Fig. 5b (etched for the longer time) is higher than in Fig. 5a. This observation leads to the conclusion that the true track density at the location shown in Fig. 5 must be at least as high as shown in Fig. 5b and therefore the lesser density should be normalized to the higher. Thus in two samples we have observed behavior which suggests that normalization is necessary.

The solar-flare differential energy spectrum is determined by choosing a trial spectrum such that the track production profile generated from the trial spectrum in our judgement best fits the experimental data. The track production profile is given analytically by the expression (Fleischer *et al.*, 1967; Maurette *et al.*, 1968):

$$\frac{d\rho(D)}{dt} = \int\int_{R}^{R+\overline{\Delta R}} \frac{dN}{dE}\frac{dE}{dx}\bigg|_{R} (1 + F\psi R)\exp(-\psi R)\, dR\, d\Omega \qquad (1)$$

where $d\rho(D)/dt$ is the number of tracks per unit area per unit time as a function of depth $D$;

$R = R(D, \theta, \phi)$ is the distance from the point of observation to the rock surface along the particle trajectory. The explicit form of $R$ is determined by geometry;

$dN/dE$ is the differential energy spectrum;

$dE/dx$ is the stopping power for iron-group nuclei in plagioclase;

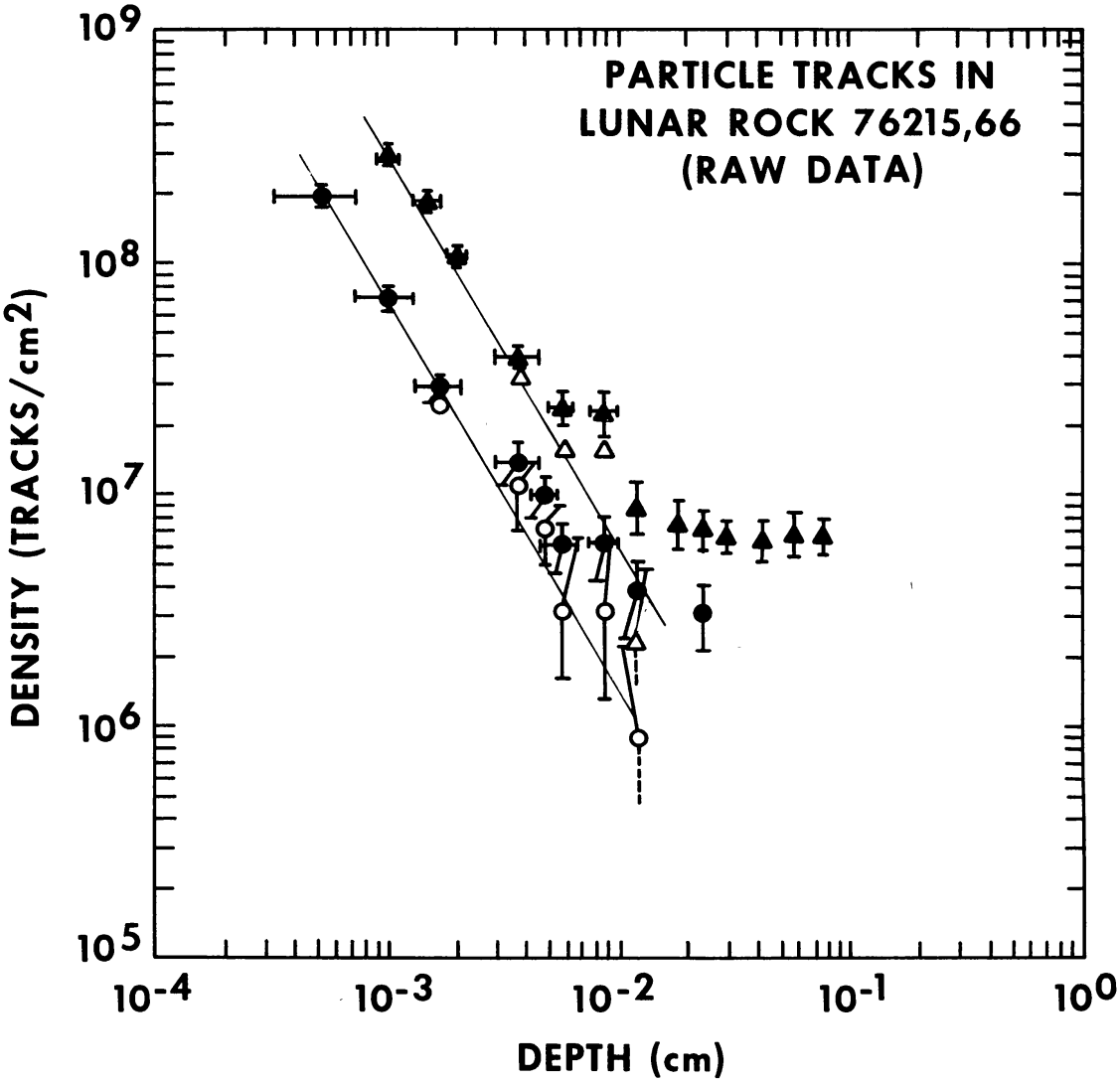


Fig. 4. Densities of particle tracks at different depths in sample 76215. Solid circles correspond to measurements made after etching 2.25 hr and solid triangles after etching 6 hr. Open symbols are determined by subtracting the galactic cosmic-ray background from the corresponding data represented by solid symbols. Lines with slopes of −1.7 are shown in order to indicate how well these data correspond to the slope of the track profile measured in 64455.

$\overline{\Delta R} = \sum A_i \Delta R_i$ is the mean etchable track length interval where the sum is over the iron-group, $A_i$ being the abundance of the $i$th ion relative to the iron-group and $\Delta R_i$ is the etchable track length interval of the $i$th ion;

$F$ is the fragmentation parameter giving the probability of a fragmented iron-group nucleus remaining in the iron-group;

$\psi = 1/\lambda$ is the reciprocal of the interaction mean free path averaged for the iron-group;

$d\Omega = \dfrac{\boldsymbol{R} \cdot d\boldsymbol{a}}{|R|^3}$ is the differential of solid angle given by the projection of the differential area onto the plane of observation divided by the square of the distance.

(a)

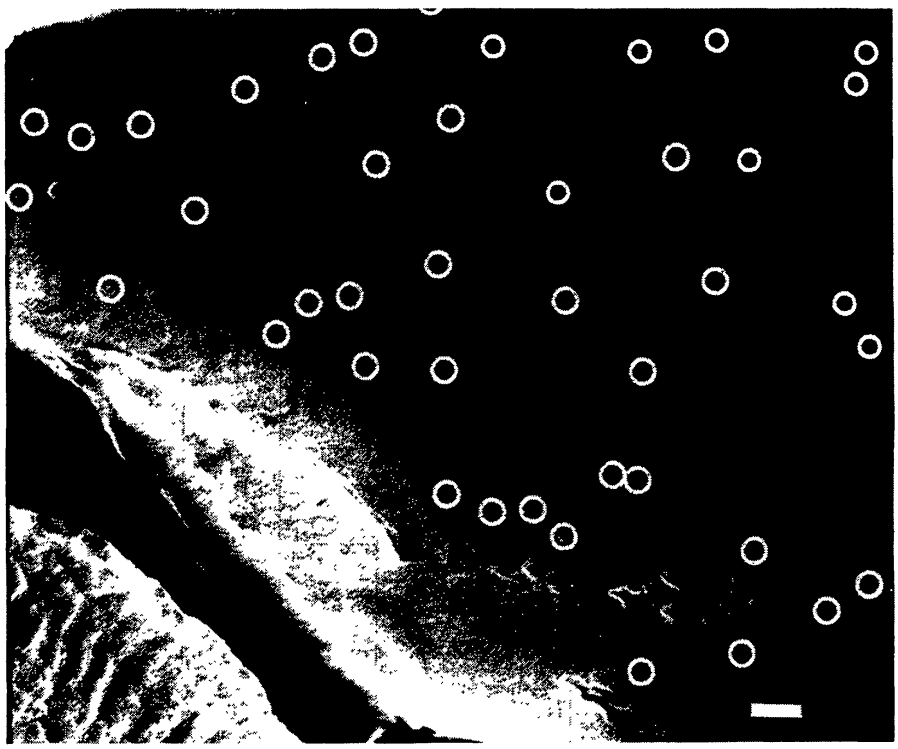

(b)

Fig. 5. Scanning electron photomicrographs of one measured location on sample 76215. The photo-mosaic (a) was taken at 10,500× after etching 2.25 hr. It has 38 tracks in an area of $3.8 \times 10^{-6}$ cm$^2$ for a density of $1.0 \pm .2 \times 10^7$ tracks/cm$^2$. The photograph (b) was taken at 5900× after etching 6 hr. It has 55 tracks (some were accidently left unmarked) in an area $2.2 \times 10^{-6}$ cm$^2$ for a density of $2.4 \pm .4 \times 10^7$ tracks/cm$^2$.

In applying this equation we have taken the stopping power $dE/dx$ and range energy relation determined from a computer program developed by Steward (1968), the first-order fragmentation parameter $F$ as 0.14 (Yuhas, 1974), and the interaction mean free path $\lambda$ as 20.6 g/cm$^2$ (Yuhas, 1974). For $D \gg R$, Eq. (1) reduces to the expression

$$\frac{d\rho(D)}{dt} = \int \frac{dN}{dE}\frac{dE}{dx}\bigg|_R \overline{\Delta R}(1 + F\psi R)\exp(-\psi R)\, d\Omega. \tag{2}$$

A very important quantity which must be determined before applying Eq. (1) is the etchable track length interval $\overline{\Delta R}$. Because the sum $\Sigma A_i \Delta R_i$ is dominated by $\Delta R_{Fe}$, it is this latter quantity which must be measured. In order to understand what we must measure we must consider the nature of the tracks. When a crystal is polished for etching, fossil tracks will be intersected arbitrarily at different points along their trajectories. For a given set of etching conditions and observational techniques, some of these tracks will be revealed and others will not. Ordinarily a criterion of track length $L$ or diameter is used by an observer in order to obtain consistent measurements and this criterion determines a value of $L_{min}$ for the shortest tracks that will be counted. The set of tracks defined by $L_{min}$ is made up of two classes. The first class consists simply in those tracks which were cut a distance $L_{min}$ from the end of their range and have etched to the end of their range; for this class we have the relation $L_{min} = R_{min}$. The other class consists of those tracks which were cut far enough from the end of their range so that they have the lowest etch rates and have just become revealed. Because etching rates vary monotonically with inverse residual range, this second class of tracks consists of tracks with the longest residual range $R_{max}$. Because all tracks intersected with ranges $R$ satisfying the relation $R_{min} \leq R \leq R_{max}$ will be revealed, the etchable track length interval $\Delta R_{Fe}$ is given by the relation $\Delta R_{Fe} = R_{max} - R_{min}$. Determination of $\Delta R_{Fe}$ requires the determination of $R_{max}$.

It would be desirable to determine $R_{max}$ using accelerated heavy ions for irradiation of plagioclase of the same composition as lunar material (Storzer *et al.*, 1973). In this way the highest energy particles to produce tracks of length $L_{min}$ under standard etching and observing conditions would determine $R_{max}$. Unfortunately, tracks exposed to the lunar environment have a special "annealed-stabilized" character which has not been successfully duplicated in the laboratory (Plieninger and Krätschmer, 1972; Burnett *et al.*, 1972; Borg *et al.*, 1973; Price *et al.*, 1973; Maurette and Price, 1975). Artificially produced particles form longer tracks that anneal quickly compared to lunar tracks and consequently this method tends to give overestimates of $R_{max}$.

Another method of determining $\Delta R_{Fe}$ is by prolonging the etching time in order to directly measure $R_{max}$ (Hutcheon *et al.*, 1974). During sequential etching steps, one must follow marked tracks which originally have a length $L_{min}$. Some of these will grow no further (the first class) and others will grow fairly long with the length of the longest track defining $R_{max}$. However, as etching is prolonged the tracks begin to overlap, especially at densities typically encountered in lunar rocks, and

following marked tracks becomes practically impossible. Hutcheon *et al.* (1974) did not actually follow marked tracks and there is no guarantee therefore that their measured maximum length $R_{max} = 40\ \mu m$ actually represents a track of length $L = L_{min}$ at the point in the etching sequence where the counted tracks were used to determine the track density. Even though they do not observe an increase in track density after subsequent etching, the tracks could be overlapping and thereby give a low track count. When not using marked tracks, the long lengths some tracks may reach will give an overestimate of $R_{max}$ and $\Delta R_{Fe}$.

The method for finding $R_{max}$ employed by Walker and Yuhas (1973) is to set the maximum track length to $R_{max}$. Yuhas (1974) selected twice the average track length for $R_{max}$. These methods have merit in attaching the value of $\overline{\Delta R}$ to the experimental conditions employed to determine track densities. However, the maximum track length is the lower limit of the value one would expect for $R_{max}$ and, therefore, these methods tend to give underestimates of $\overline{\Delta R}$. A thorough discussion on this point is given by Yuhas (1974) who demonstrates that setting $L_{max} = R_{max}$ results in a value probably no less than 20% of the true value of $R_{max}$ because: (1) for typical etching conditions measured track densities approach a limiting value with increased etching time and (2) maximum track lengths average about $10.5\ \mu m \pm 20\%$ in feldspars (Price *et al.*, 1973). Therefore, we have adopted this procedure for determining $\overline{\Delta R}$.

In order to determine a differential energy spectrum and track production profile of the greatest general utility, we have chosen a trial spectrum that produces a track production profile which fits the data in sample 64455 from 1 to 700 $\mu$m and which fits the data in sample 68815, a rock with an identical krypton exposure age (Walker and Yuhas, 1973), at depths greater than 2 cm. The intermediate spectrum is chosen to smoothly connect between the two with reasonable agreement between both sets of data. This is not the same as connecting the solar-flare spectrum determined from 64455 smoothly to the Walker and Yuhas spectrum (1973) because a different density is used for 68815 ($2.8\ g/cm^3$) and the Surveyor glass spectrum used for the solar-flare region by Walker and Yuhas (1973) will not smoothly connect to the spectrum used to fit sample 64455.

In deriving a track production curve from Eq. (2) to fit our data we used a value of $\overline{\Delta R} = 9\ \mu m$ derived from $L_{min} = 2\ \mu m$ and $L_{max} = 11\ \mu m$. We consider it appropriate for us to use Eq. (2) rather than Eq. (1) because the value of $\overline{\Delta R} = 9\ \mu m$ is strictly valid only for the points marked as solid diamonds in Fig. 2. Our interpretation of the normalization factors used to obtain Fig. 3 from Fig. 2 is that they are based on variations in $\Delta R$. The column of estimated $\Delta R$ in Table 1 is obtained by dividing 9 $\mu$m by the normalization factor attributed to variations in $\overline{\Delta R}$. It is apparent that estimated values of $\overline{\Delta R}$ are always much less than $D$ for any given data set, and consequently Eq. (2) rather than Eq. (1) can be used. If we used the values of $\overline{\Delta R}$ given in Table 1 and calculated profiles using Eq. (1), we would obtain a segmented "track profile" to use with Fig. 2. However, this is circular reasoning and it was not the actual procedure we followed. Appropriate limits of integration for solid angle were taken in Eq. (2) to correspond to a zenith

angle of 80° (Yuhas, 1974). In Fig. 3 we show what we believe to be the best fit to our data where the upper curve applies to a radius of curvature of 0.9 cm and that below to an infinite plane. Because the sample was partially buried in the regolith, the track profile should show the effect of the soil line and apparently does so at depths greater than ~3 mm. The high density of tracks from .5 to 2 mm arises from the fact that there are small spall zones which acutely affect track densities at these depths especially along the radii on which these measurements were made (Figs. 1 and 2). Unfortunately, the disposition of suitable crystals made the choice of these radii mandatory. The rise in densities with depth in sample 64455,16 at depths greater than 1 cm is probably not statistically significant.

Sample 76215 was examined expressly to determine whether or not erosion (or shielding by a thin dust cover) affected the track density versus depth profile of 64455. As previously mentioned, 76215 was exposed for a short period and the surfaces exposed at the time of collection showed no erosion. We selected a sample from 76215 (after SEM examination to determine crater densities, uniformity of patination, etc.) for which erosion by micrometeoroid impact was negligible. The track density versus depth profile for 76215 is identical to that observed in 64455 (cf. Figs. 3 and 4), therefore we conclude that the profile in 64455,14 was not significantly affected by either erosion or shielding by dust.

The differential energy spectrum used to obtain the track profiles in Figs. 3 and 6 is given by the solid line in Fig. 7 and is our best estimate of the $2 \times 10^6$ yr average spectrum for iron-group nuclei. In fitting the data for 68815 of Walker and Yuhas (1973) we have used the revised value $R_{max} = 9.8$ $\mu$m from Yuhas (1974) to obtain $\overline{\Delta R} = 7.8$ $\mu$m. In Fig. 6 we show what we believe to be the best fit to their

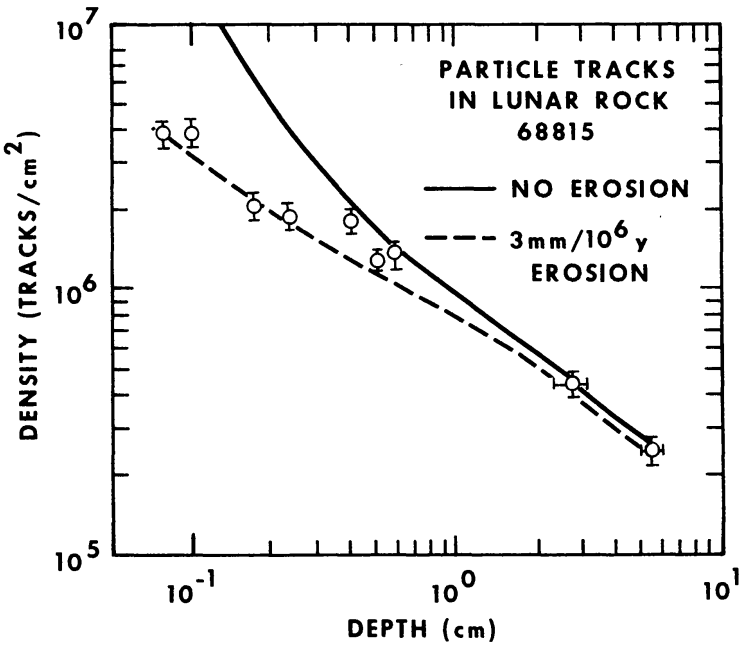


Fig. 6. Track density profile derived for sample 68815 for no erosion and for 3 mm/$10^6$-yr continuous infinitesimal erosion. Track densities were measured by Walker and Yuhas (1973).

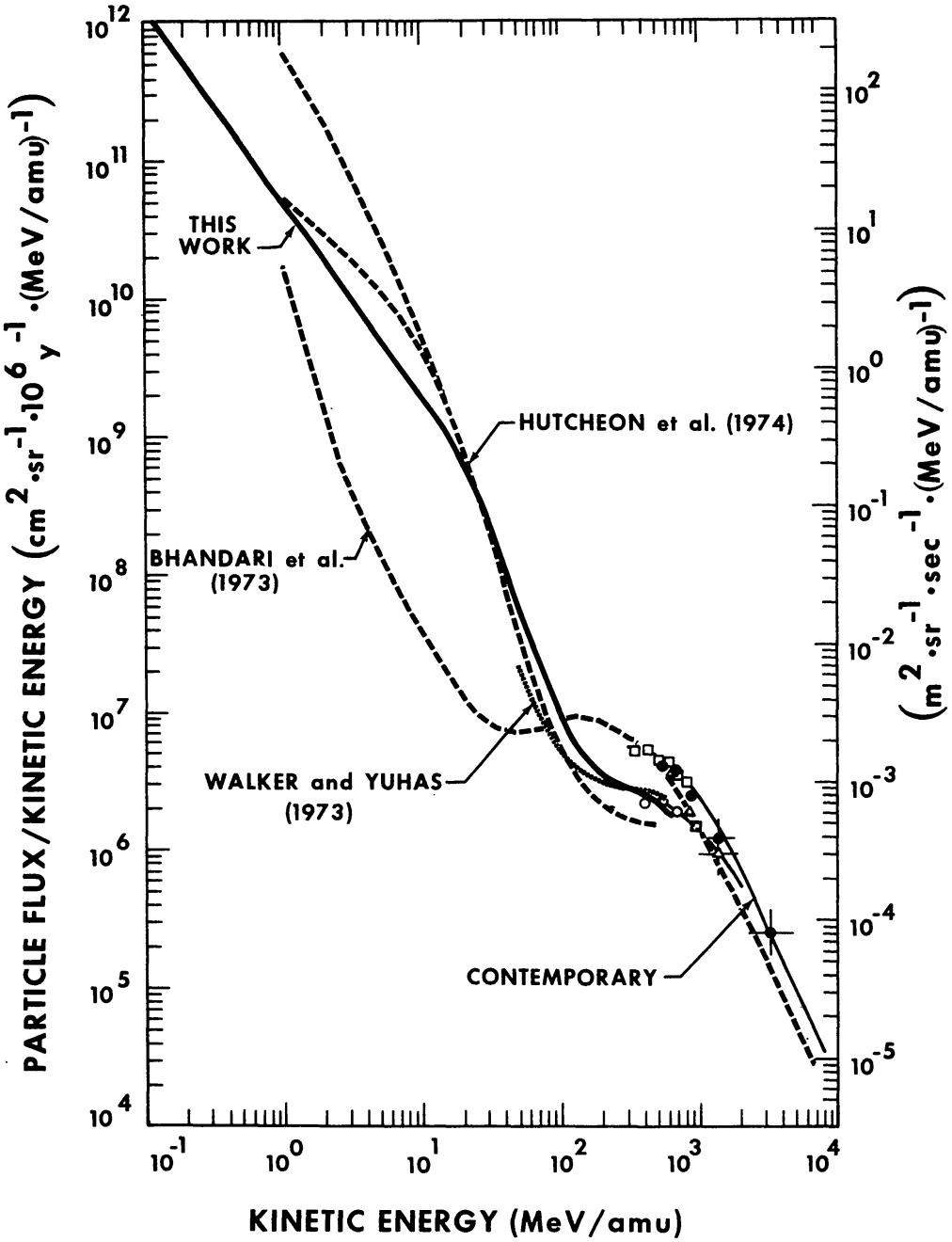


Fig. 7. Differential energy spectrum of iron-group nuclei derived here together with other recent measurements by Bhandari *et al.* (1973), Walker and Yuhas (1973), and Hutcheon *et al.* (1974) and a summary of recent non-track measurements marked "contemporary." The data shown for the contemporary galactic cosmic-ray flux are from Webber and Ormes (1967) (solid circles), Freier and Waddington (1968) (open squares), Von Rosenvinge *et al.* (1969) (open triangles), and Cleghorn *et al.* (1971) (open circles).

data. The fitting of the solar-flare spectrum derived from sample 64455 to the 68815 data requires a 2.5–3 mm/$10^{6}$-yr erosion rate for the latter in order to fit all points. This does not imply that the average lunar erosion rate by mass wastage is as high as 2.5–3 mm/$10^{6}$ yr. This erosion rate could be real but localized, or an artifact of the computation because our calculational method assumes continuous

infinitesimal erosion. Discrete erosional processes would lead to a lower value (Yuhas, 1974). A localized erosion as high as 3 mm/$10^6$ yr would be consistent with estimates from the Monte Carlo calculations of Hörz *et al.* (1974).

We may ask, if samples 64455 and 68815 are both South Ray Crater ejecta with an exposure age of $2 \times 10^6$ yr, why 68815 appears to be highly eroded and 64455 has areas that are uneroded. The answer appears to be providence. First, 64455 is eroded, which can be seen in Fig. 1 with an average erosion rate $\geqslant$0.25 mm/$10^6$ yr for zenith angles less than 40°. This value is identical to that predicted by Hörz *et al.* (1974) for flux III. The zenith angle of 45° determined for 68815 can be smaller (Yuhas, personal communication) and, therefore, we may be comparing areas that are not strictly comparable in terms of their exposure geometry. The difference in apparent erosion rates may result from differences in the strength of the glass and the anorthosite (Vedder, 1971), chipping during sampling or in sample handling, or simply a statistical fluctuation. The difference is not large enough to be considered significant.

## DISCUSSION

### (a) *Comparison to other results*

It is of interest to compare long-term solar-flare spectrum determinations with the short-term measurements provided by Surveyor 3. The spectrum derived from the Surveyor 3 glass filter (Crozaz and Walker, 1971; Fleischer *et al.*, 1971; Price *et al.*, 1971) is not explicitly shown in Fig. 7 because the magnitude of this spectrum must be determined by external parameters. There is no reason *per se* that the Surveyor spectrum should agree with the long-term average, especially considering that the Surveyor period included no large flares. Nevertheless, the most recent reappraisal of the Surveyor measurements by Hutcheon *et al.* (1974) indicates that it is essentially identical to their long-term ($\sim 10^5$-yr) spectrum from about 20 to 80 MeV/a.m.u. For example, Hutcheon *et al.* (1974) show that the solar-flare exposure age for sample 72315 determined assuming a spectrum of the Surveyor type ($3.2 \times 10^5$ yr) is in good agreement with the galactic cosmic-ray exposure age determined for the same rock by fitting the galactic track profile measured to the Walker and Yuhas (1973) galactic spectrum ($2.2 \times 10^5$ yr). Our spectrum is also approximately parallel to the Surveyor glass spectrum from 35 to 70 MeV/a.m.u. (500 $\mu$m–2 mm). It is higher by a factor of $\sim$2.4 over this range than the spectrum used by Walker and Yuhas (1973) and higher by a factor of $\sim$1.5 compared to the reappraised Surveyor spectrum evaluated by Hutcheon *et al.* (1974).

Comparison of our spectrum to that of Hutcheon *et al.* (1974) looks fairly good in Fig. 7. Their lower curve was determined directly from sample 72315, whereas the upper curve was determined by extending the 72315 data to agree in spectral shape with measurements in a vug crystal in sample 15499 (Hutcheon *et al.*, 1972). In view of other recent measurements in lunar rocks at depths less than 80 $\mu$m these workers conclude that the solar-flare spectrum may be flatter than indicated by the upper curve (Hutcheon, 1975). Therefore, we will restrict our comparison to the

lower curve. The general trend in both is a relatively flat slope from 0.1 to 10 MeV/a.m.u. which then steepens to a slope of approximately −3, as in the Surveyor glass, to about 70 MeV/a.m.u. In our case the slope of −1.4 from 0.1 to ~15 MeV/a.m.u. is steeper than that of Hutcheon *et al.* (1974). Their somewhat flatter spectrum may result from experimental techniques in a manner that is discussed below.

Even though the overall spectral shapes determined by Hutcheon *et al.* (1974) and ourselves are comparable, there is a difference in production rate not brought out in Fig. 7. We have used a value of $\overline{\Delta R} = 9$ μm, whereas Hutcheon *et al.* (1974) use a value of $\overline{\Delta R} = 40$ μm. Consequently if we compare track production profiles, their spectrum would be approximately 6 times higher than ours at 50 MeV/a.m.u. Because the true value of $\overline{\Delta R}$ is not likely to be very different for either experiment, the discrepancy in magnitude is very large and is understandable only if the solar-flare exposure age of 72315 is considerably higher than $3 \times 10^5$ yr.

Comparison of the track determined solar-flare–galactic cosmic-ray energy spectrum to contemporary measurements shows an interesting trend. The contemporary measurements in Fig. 7 show two curves, the higher of which is from measurements taken at solar minimum, whereas the lower represents measurements taken near solar maximum during solar cycle 20. These excursions result from modulation of the galactic cosmic rays in the solar cavity, an effect correlated to solar activity. The long-term average spectra determined by Walker and Yuhas (1973) and this work agree best with data taken near solar maximum which implies that the average solar activity over time scales of $2 \times 10^6$ yr is similar to that of solar maximum in cycle 20. Even though the adopted criterion for $\overline{\Delta R}$ does not permit an absolute comparison to non-track data, the absolute value of $\overline{\Delta R}$ must be larger rather than smaller than that used by Walker and Yuhas (1973) and by us which would lower the spectra and add weight to our claim. The Hutcheon *et al.* (1974) spectrum, as it stands, would also support this claim, but if it is corrected by a factor of four to correlate to our value of $\overline{\Delta R}$, their spectrum would agree with minimum modulation during solar cycle 20. The spectrum of Bhandari *et al.* (1973), which for the galactic spectrum depends on the measurements of Lal *et al.* (1969) in the meteorite St. Séverin, agrees better with lower solar modulation. As observed by Lal *et al.* (1969), this is compatible with a theoretically lower solar modulation at 2–3 a.u., the presumed mean orbital distance for St. Séverin. The solar-flare spectrum of Bhandari *et al.* (1973) disagrees with other measurements most probably because it relies on data from eroded lunar rocks.

Solar cycle 20 was a cycle of average solar activity when compared to the accurate records of sunspot numbers for the last 220 yr (Dodson *et al.*, 1974), if solar activity is defined by sunspot number. If our observation is confirmed, however, the average cycle for the last 220 yr is lower than the $2 \times 10^6$-yr average. However, we are comparing our data to contemporary data that was taken several years before the observation of the most intense flares in cycle 20 and consequently the long-term data may actually be more compatible to the present-day average rather than the present-day maximum. Of course there could be many large fluctuations in solar activity on time scales to which we are insensitive.

(b) *Track production profile*

In Fig. 8 we show the track production profile below an infinite plane rock surface perpendicular to the zenith for an observational surface parallel to the rock surface ($\beta = 0°$) and perpendicular to the rock surface ($\beta = 90°$) derived from our

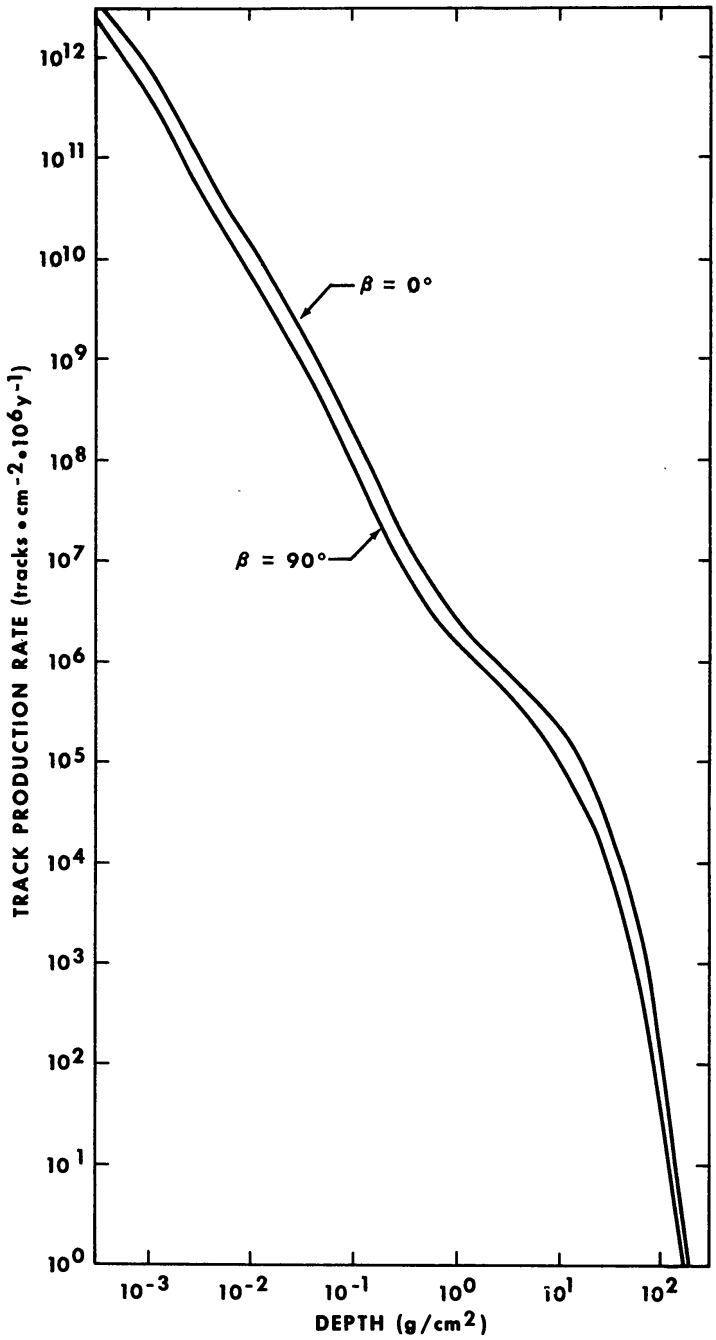


Fig. 8. Track production profiles below an infinite plane rock surface at 0° zenith angle and for observational surfaces parallel ($\beta = 0°$) and perpendicular ($\beta = 90°$) to the rock surface. These curves are derived for a $10^6$-yr exposure period, $\overline{\Delta R} = 10$ $\mu$m, and for no erosion. They can be used to determine solar-flare track exposure ages under conditions described in the text.

spectrum in Fig. 7. These standard profiles are derived using $\overline{\Delta R} = 10\ \mu m$ and a time period of $10^6$ yr. These profiles can be used to determine solar-flare track ages under the following conditions:

(1) The depth $D$ at which a measurement is made is much less than the effective radius of curvature of the sample.
(2) $\overline{\Delta R}$ is much less than $D$ and the track production profile is corrected by $\overline{\Delta R}/10\ \mu m$.
(3) The erosional depth is very much less than $D$.
(4) For measurements made in substances other than plagioclase the profiles are corrected by multiplying by the relative etching efficienty $\alpha$ of that substance to plagioclase. We take the etching efficiency of plagioclase to be 1.
(5) For an observational surface at an angle $\beta$ relative to the rock surface, the track production profile $\Phi(D, \beta)$ is taken as

$$\Phi(D, \beta) = \Phi(D, 0°) \cos^2 \beta + \Phi(D, 90°) \sin^2 \beta.$$

(6) For zenith angles other than 0° the track production profile is corrected by the factor taken from Fig. 9.

In other cases, the energy spectra given in Fig. 7 should be used in Eq. (1) and the particular production profile applicable to the sample should be derived. This calculation should also take into consideration erosional effects (Yuhas, 1974). Two further points should be kept in mind for depths less than ~100 $\mu$m (or $E \lesssim 10$ MeV/a.m.u.). For typical lunar rocks, exposure ages are long enough so

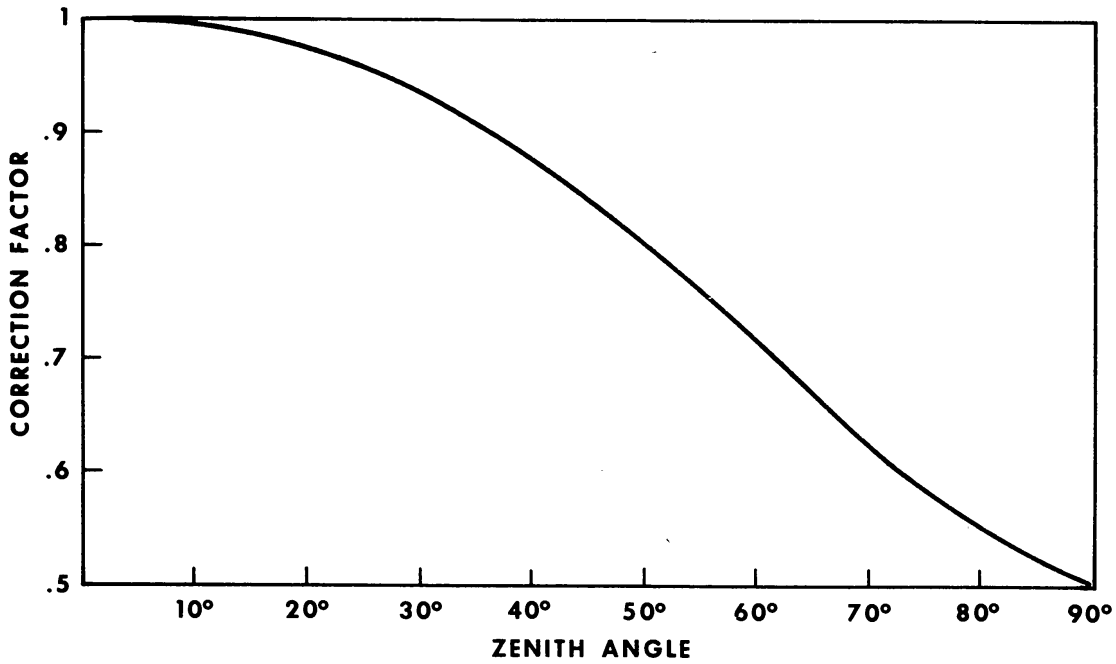


Fig. 9. Correction factors to be applied to the track production profiles in Fig. 8 for rock surfaces exposed at different zenith angles.

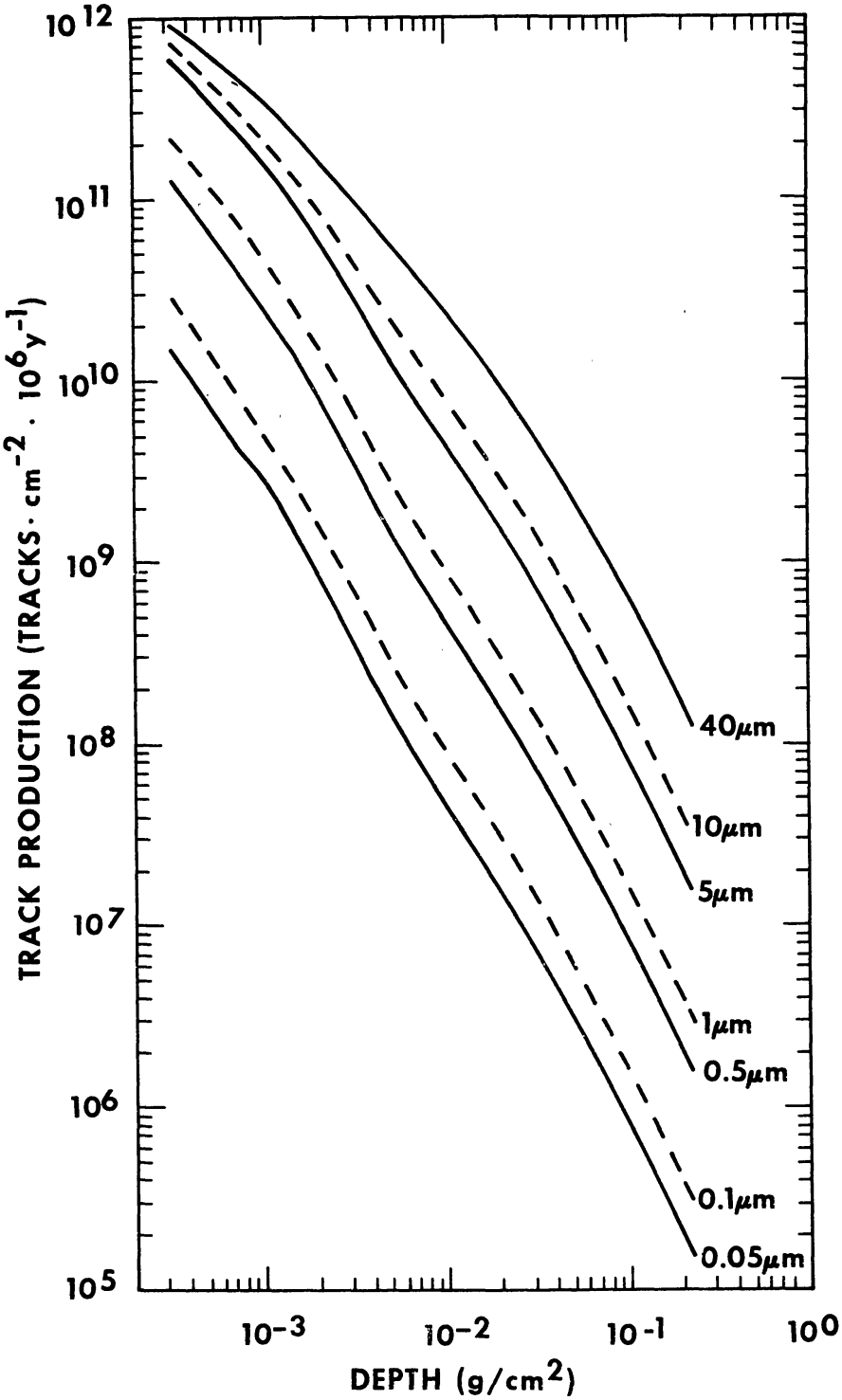


Fig. 10. Track production profiles down to $2 \times 10^{-1}$ g/cm$^2$ as a function of different values of $\overline{\Delta R}$. The profiles not only increase in magnitude with increasing $\overline{\Delta R}$ but also have flatter slopes.

that very high track densities develop. Even with the best presently available techniques tracks will overlap at densities of $10^{10}$–$10^{11}$ tracks/cm$^2$ and measured profiles will be flatter than the profiles in Fig. 8. There is, in addition, an inherent flattening of the spectrum when $\overline{\Delta R}$ is not much greater than $D$, which is when Eq. (1) rather than Eq. (2) is applicable. Using Eq. (1) we have derived the production profile for different values of $\overline{\Delta R}$ which are shown in Fig. 10. It is apparent from this graph that the shape as well as the magnitude vary with $\overline{\Delta R}$, with larger values of $\overline{\Delta R}$ leading to flatter profiles. If very short etching times are used such that Eq. (2) can be applied then normalization of the data will be required; for longer etching times, when it is appropriate to apply Eq. (1), normalization may not be required, but the track profile will be flatter than in the first case.

The $2 \times 10^6$ yr average differential energy spectrum derived from track densities in sample 64455 should provide a reliable standard with which to compare other track density measurements. Because our data at depths 1–4 mm seems to be affected by erosion and deeper points are affected by the soil line, it should be possible to resolve the spectral shape more accurately from 40 to 150 MeV/a.m.u. by track profile measurements in other samples.

*Acknowledgments*—One of us (GB) gratefully acknoweldges support by the National Research Council as a Resident Research Associate at the NASA Johnson Space Center during the time most of this work was done. We wish to thank J. N. Goswami and E. Zinner for very constructive reviews and E. Stockton for manuscript preparation. This is Lunar Science Institute contribution 232.

## References

ALGIT (Apollo Lunar Geology Investigation Team) U.S. Geological Survey (1973) Preliminary geologic analysis of the Apollo 17 site. *Interagency Report: Astrogeology* **72**, U.S. Geol. Survey, March 17.

Behrman C., Crozaz G., Drozd R., Hohenberg C. M., Ralston C., Walker R. M., and Yuhas D. (1973) Cosmic ray exposure history of North Ray and South Ray material. *Proc. Lunar Sci. Conf. 4th*, p. 1957–1974.

Bhandari N., Goswami J. N., Lal D., and Tamhane A. S. (1973) Charge composition and energy spectrum of solar flare and VVH and VH nuclei. Proc. Thirteenth Int. Cosmic Ray Conf., Vol. 2, pp. 1464–1469. University of Denver.

Blanford G. E., Fruland R. M., McKay D. S., and Morrison D. A. (1974) Lunar surface phenomena: Solar flare track gradients, microcraters, and accretionary particles. *Proc. Lunar Sci. Conf. 5th*, p. 2501–2526.

Borg J., Dran J. C., Comstock G., Maurette M., Vassent B., Duraud J. P., and Legressus C. (1973) Nuclear particle track studies in the lunar regolith—some new trends and speculations (abstract). In *Lunar Science IV*, p. 82–84. The Lunar Science Institute, Houston.

Burnett D., Hohenberg C. M., Maurette M., Monnin M., Walker R., and Woolum D. (1972) Cosmic ray solar wind, solar flare, and neutron albedo measurements. In *Apollo 16 Preliminary Sci. Report*, Nasa publication SP-315, pp. 15-19 to 15-32.

Cleghorn T. F., Freier P. S., and Waddington C. J. (1971) On the modulation and energy spectrum of highly charged cosmic ray nuclei. *Astrophys. Space Sci.* **14**, 422–430.

Crozaz G. and Walker R. M. (1971) Solar particle tracks in glass from Surveyor 3. *Science* **171**, 1237–1239.

Crozaz G., Walker R., and Woolum D. (1971) Nuclear track studies of dynamic surface processes on the moon and the constancy of solar activity. *Proc. Lunar Sci. Conf. 2nd*, p. 2543–2558.

Dodson H. W., Hedeman E. R., and Mohler O. C. (1974) Comparison of activity in solar cycles 18, 19, and 20. *Rev. Geophys. Space Phys.* **12**, 329–341.

Drozd R. J., Hohenberg C. M., Morgan C. J., and Ralston C. E. (1974) Cosmic-ray exposure history at the Apollo 16 and other lunar sites: Lunar surface dynamics. *Geochim. Cosmochim. Acta* **38**, 1625–1642.

Fleischer R. L., Price P. B., Walker R. M., and Maurette M. (1967) Origins of fossil charged particle tracks in meteorites. *J. Geophys. Res.* **72**, 331–353.

Fleischer R. L., Hart H. R., and Comstock G. M. (1971) Very heavy solar cosmic rays: Energy spectrum and implications for lunar erosion. *Science* **171**, 1240–1242.

Freier P. S. and Waddington C. J. (1968) Very heavy nuclei in the primary cosmic radiation. I. Observations on the energy spectrum. *Phys. Rev.* **175**, 1641–1648.

Hörz F., Schneider E., and Hill R. E. (1974) Micrometeoroid abrasion of lunar rocks: A Monte Carlo simulation. *Proc. Lunar Sci. Conf. 5th*, p. 2397–2412.

Hutcheon I. D. (1975) Micrometeorites in and out of the plane of the ecliptic. To be published.

Hutcheon I. D., Braddy D., Phakey P. P., and Price P. B. (1972) Study of solar flares, cosmic dust and lunar erosion with vesicular basalts. In *The Apollo 15 Lunar Samples* (editors J. Chamberlain and C. Watkins), p. 412–414. The Lunar Science Institute, Houston.

Hutcheon I. D., Macdougall D., and Price P. B. (1974) Improved determination of the long-term average Fe spectrum from 1 to 460 MeV/a.m.u. *Proc. Lunar Sci. Conf. 5th*, p. 2561–2576.

Lal D., Lorin J. C., Pellas P., Rajan R. S., and Tamhane A. S. (1969) On the energy spectrum of iron-group nuclei as deduced from fossil-track studies in meteorite minerals. *Meteorite Research* (editor P. M. Millman), p. 275–285. D. Reidel.

Maurette M. and Price P. B. (1975) Electron microscopy of irradiation effects in space. *Science* **187**, 121–129.

Maurette M., Thro P., Walker R., and Webbink R. (1969) Fossil tracks in meteorites and the chemical abundance and energy spectrum of extremely heavy cosmic rays. In *Meteorite Research* (editor P. M. Millman), p. 286–315. D. Reidel.

Morrison D. A. and Zinner E. (1975) Studies of solar flares and impact pits in partially protected crystals. *Proc. Lunar Sci. Conf. 6th.* This volume.

Plieninger T. and Krätschmer W. (1972) Registration properties of pyroxenes for various heavy ions and consequences to the determination of the composition of the cosmic radiation. Eight Int. Conf. on Nuclear Photog. and Solid State Track Detectors, Bucharest.

Price P. B., Hutcheon I. D., Cowsik R., and Barber D. J. (1971) Enhanced emission of Fe nuclei in solar flares. *Phys. Rev. Lett.* **26**, 916-919.

Price P. B., Lal D., Tamhane A. S., and Perelygin V. P. (1973) Characteristics of tracks of ions with $14 \leq Z \leq 36$ in common rock silicates. *Earth Planet. Sci. Lett.* **19**, 377–395.

Schneider E. and Hörz F. (1974) Microcrater populations on Apollo 17 rocks. *Icarus* **22**, 459–473.

Steward P. G. (1968) Stopping power and range for any nucleus in the specific energy interval 0.01 to 500 MeV/a.m.u. in any nongaseous material. Ph.D. thesis, University of California, Berkeley.

Storzer D., Poupeau G., and Krätschmer W. (1973) Track-exposure and formation ages of some lunar samples. *Proc. Lunar Sci. Conf. 4th*, p. 2363–2377.

Vedder J. F. (1971) Microcraters in glass and minerals. *Earth Planet. Sci. Lett.* **11**, 291–296.

Von Rosenvinge T. T., Webber W. R., and Ormes J. F. (1969) A comparison of the energy spectra of cosmic ray helium and heavy nuclei. *Astrophys. Space Sci.* **5**, 342–359.

Walker R. and Yuhas D. (1973) Cosmic ray production rates in lunar materials. *Proc. Lunar Sci. Conf. 4th*, p. 2379–2389.

Webber W. R. and Ormes J. F. (1967) Cerenkov-scintillation counter measurements of nuclei heavier than helium in the primary cosmic radiation. 1. Charge composition and energy spectra between 200 MeV/nucleon and 5 GeV/nucleon. *J. Geophys. Res.* **72**, 5957–5976.

Yuhas D. E. (1974) The particle track record in lunar silicates: Long-term behavior of solar and galactic VH nuclei and lunar surface dynamics. Ph.D. thesis, Washington University, St. Louis.